Calorimetric and Dielectric Studies on the Water Reorientation in the Two-Dimensional Hydrogen-Bond System of $Cd(H_2O)_2Ni(CN)_4 \cdot 4H_2O$ Crystal†

Kenji Okishiro, Osamu Yamamuro,* Itaru Tsukushi,‡ and Takasuke Matsuo

Department of Chemistry and Microcalorimetry Research Center, Graduated School of Science, Osaka University, 1-1 Machikaneyama-cho, Toyonaka, Osaka 560, Japan

Shin-ichi Nishikiori and Toschitake Iwamoto§

Department of Basic Science, Graduate School of Arts and Sciences, The University of Tokyo, Komaba, Meguro, Tokyo 153, Japan

Received: February 28, 1997; In Final Form: May 20, 1997⊗

The heat capacity of $Cd(H_2O)_2Ni(CN)_4 \cdot 4H_2O$ crystal in which the water molecules form a two-dimensional quasi-hexagonal hydrogen-bond network was measured with an adiabatic calorimeter in the temperature range 5−300 K. A glass transition due to the freezing of the reorientational motion of the water molecules was found around 120 K. The reorientational relaxation times were obtained from the enthalpy relaxation data around the glass transition. The complex dielectric permittivity was also measured in the temperature range 150−285 K and in the frequency range 20 Hz−1 MHz. A dielectric dispersion associated with the reorientational motion of the water molecules was observed in the temperature range 160−270 K. The dielectric relaxation times were calculated from the temperature and frequency dependence of the ϵ'' data. Calorimetric and dielectric relaxation times lie on separate smooth lines in the wide time scale over $10^{-6}-10^{6}$ s in the Arrhenius plot. The mechanism of the water reorientational motion was discussed on the basis of the model considering the formation and transfer of the Bjerrum defect as in the case of the three-dimensional ice polymorphs.

1. Introduction

There are a number of hydrate crystals in which the water molecules form various types of hydrogen-bond networks.[1,2] $SnCl_2 \cdot 2H_2O$ and $Cu(HCO_2)_2 \cdot 4H_2O$ have attracted the special attention of physical chemists since these crystals can be regarded as "two-dimensional ice". The structural studies[3−6] have shown that the water molecules form hydrogen-bond networks in a layer and are orientationally disordered while satisfying the "ice rules",[7] i.e., one proton is located on an O−H···O hydrogen bond and two protons are bonded to one oxygen atom so as to maintain an electrical neutral condition. The structure of the H_2O layer of $SnCl_2 \cdot 2H_2O$[3,4] consists of four-membered and eight-membered rings of oxygen atoms, while that of $Cu(HCO_2) \cdot 4H_2O$[5,6] of only six-membered rings. In both compounds, a part of the protons of H_2O make static hydrogen bonds to the atoms of the neighboring layers, i.e., to the chlorine atoms of the $SnCl_2$ layer or to the oxygen atoms of the formic acid layer. Our heat capacity measurements have revealed that $SnCl_2 \cdot 2H_2O$[8−11] and $Cu(HCO_2)_2 \cdot 4H_2O$[12] undergo a phase transition due to the orientational ordering at 218 and 234 K, respectively.

The present compound $Cd(H_2O)_2Ni(CN)_4 \cdot 4H_2O$, which was synthesized in 1993,[13,14] also has a two-dimensional hydrogen-bonded network. The X-ray diffraction study has revealed that this crystal belongs to the space group *Pnma* (no. 62) and consists of the $Cd(H_2O)_2Ni(CN)_4$ and H_2O layers alternating along the *a* axis; two of the H_2O in the molecular formula are coordinated to the Cd atom and four involved in the H_2O network layer. The network of water molecules consists of larger and smaller hexagons of the water molecules; one hexagon is surrounded by the other six hexagons sharing each edge. Though the position of the protons has not be determined, it is likely that the orientation of the water molecules are disordered while satisfying the ice rule. Some protons may be located out of the H_2O layer, not bonded to any atoms of the $Cd(H_2O)_2Ni(CN)_4$ layer. Such non-hydrogen-bonded protons do not exist in the two-dimensional system of $SnCl_2 \cdot 2H_2O$ and $Cu(HCO_2)_2 \cdot 4H_2O$. We suppose that these protons considerably affect the thermodynamic and kinetic properties of the hydrogen-bond system. Thus $Cd(H_2O)_2Ni(CN)_4 \cdot 4H_2O$ is regarded as "real two-dimensional ice" in the sense that the water molecules are not coupled strongly to the neighboring layers.

The aim of this study is to investigate the ordering process and dynamical property of the water molecules in the two-dimensional hydrogen-bond system of $Cd(H_2O)_2Ni(CN)_4 \cdot 4H_2O$. We have performed calorimetric and dielectric measurements in the wide temperature and frequency (for dielectric measurement) ranges. In the dielectric study, the temperature dependence of the relaxation time of the water reorientation can be determined since the water reorientation is accompanied by large dipole fluctuation; the dipole moment of a water molecules is 1.94 Debye. Given the positional disorder of protons in the network, a phase transition due to the ordering of the water reorientation could occur below room temperature as in the case of $SnCl_2 \cdot 2H_2O$ and $Cu(HCO_2)_2 \cdot 4H_2O$. If the relaxation time of the water reorientation, which will increase with decreasing temperature, becomes longer than the experimental time scale (ca. 10^3 s) at a temperature higher than the ordering transition temperature, a glass transition would be observed as in the cases of three dimensional ices and clathrate hydrates.

† Contribution no. 131 from the Microcalorimetry Research Center.

* Corresponding author: phone, +81-6-850-5399; fax, +81-6-850-5397; e-mail, yamamuro@chem.sci.osaka-u.ac.jp.

‡ Present address: Institute for Chemical Research, Kyoto University, Uji, Kyoto 611, Japan.

§ Present address: Department of Fundamental Science, College of Science and Engineering, Iwaki Meisei University, Chuohdai Iino, Iwaki, Fukushima 970, Japan.

⊗ Abstract published in *Advance ACS Abstracts,* July 1, 1997.

S1089-5647(97)00743-8 CCC: $14.00

TABLE 1: Experimental Molar Heat Capacities of $CdNi(H_2O)_2(CN)_4\cdot 4H_2O$ Crystal (M = 383.27 g mol^{-1}, R = 8.314 51 J K^{-1} mol^{-1})

T/K	$C_{p,m}/R$	T/K	$C_{p,m}/R$	T/K	$C_{p,m}/R$	T/K	$C_{p,m}/R$	T/K	$C_{p,m}/R$	T/K	$C_{p,m}/R$
5.92	0.08775	26.90	4.668	60.86	15.25	100.26	24.57	152.45	34.50	221.45	45.08
6.51	0.1119	27.77	4.949	62.02	15.57	101.76	24.90	154.34	34.82	223.97	45.45
6.97	0.1397	28.68	5.273	63.19	15.88	103.26	25.20	156.24	35.14	226.51	45.82
7.51	0.1719	29.67	5.620	64.35	16.18	104.78	25.52	158.30	35.48	229.06	46.19
8.11	0.2158	30.70	5.915	65.52	16.49	106.31	25.83	160.28	35.81	231.63	46.57
8.73	0.2729	31.75	6.262	66.70	16.79	107.86	26.14	162.30	36.14	234.22	46.94
9.38	0.3370	32.82	6.623	67.87	17.10	109.41	26.46	164.34	36.47	236.82	47.35
10.02	0.4115	33.89	6.987	69.05	17.40	110.98	26.77	166.39	36.80	239.44	47.79
10.64	0.4932	34.97	7.351	70.24	17.69	112.57	27.09	168.47	37.14	242.08	48.18
11.24	0.5864	36.05	7.713	71.43	18.00	114.16	27.40	170.57	37.48	244.73	48.46
11.83	0.6773	37.12	8.059	72.62	18.29	115.77	27.72	172.69	37.81	247.40	48.79
12.39	0.7696	38.19	8.411	73.82	18.59	117.39	28.05	174.82	38.14	250.08	49.15
12.94	0.8682	39.26	8.750	75.02	18.88	119.03	28.39	176.98	38.48	252.79	49.53
13.50	0.9750	40.34	9.098	76.23	19.17	120.67	28.73	179.15	38.82	255.50	49.91
14.10	1.096	41.44	9.444	77.44	19.46	122.33	29.07	181.34	39.16	258.24	50.31
14.73	1.228	42.54	9.789	78.62	19.75	124.00	29.41	183.55	39.50	260.99	50.71
15.39	1.374	43.64	10.14	79.78	20.02	125.68	29.73	185.79	39.84	263.75	51.14
16.07	1.531	44.77	10.49	80.98	20.28	127.38	30.06	188.04	40.18	266.54	51.52
16.76	1.696	45.92	10.84	82.21	20.58	129.09	30.38	190.30	40.51	269.35	51.96
17.45	1.873	47.06	11.20	83.47	20.87	130.81	30.70	192.59	40.86	272.19	52.41
18.14	2.054	48.21	11.55	84.76	21.17	132.54	31.01	194.90	41.21	275.06	52.83
18.82	2.240	49.35	11.90	86.08	21.47	134.29	31.33	197.22	41.55	277.95	53.28
19.53	2.440	50.50	12.26	87.42	21.77	136.05	31.64	199.56	41.89	280.87	53.74
20.04	2.578	51.65	12.61	88.79	22.09	137.82	31.96	201.92	42.25	283.81	54.22
20.84	2.811	52.79	12.95	90.18	22.41	139.60	32.29	204.30	42.60	286.78	54.71
21.67	3.059	53.94	13.28	91.58	22.71	141.40	32.60	206.70	42.95	289.77	55.21
22.53	3.319	55.09	13.62	93.00	23.01	143.21	32.92	209.11	43.30	292.79	55.72
23.40	3.587	56.24	13.96	94.42	23.32	145.04	33.24	211.55	43.65	295.83	56.15
24.27	3.859	57.39	14.28	95.86	23.63	146.87	33.56	214.00	44.00	298.90	56.75
25.15	4.127	58.55	14.60	97.32	23.96	148.72	33.87	216.46	44.35		
26.03	4.397	59.70	14.93	98.78	24.26	150.58	34.18	218.95	44.72		

2. Experimental Section

The sample used for the measurements was prepared by the following way. $K_2[Ni(CN)_4]\cdot H_2O$ was first prepared from $NiCl_2\cdot 6H_2O$ (98%) and KCN (98%) according to the method given in ref 15. Into 100 mL of water were added 15 mmol each of $CdCl_2\cdot 2.5H_2O$ (99.9%, 3.40 g) and $K_2[Ni(CN)_4]\cdot H_2O$ (3.90 g) and 11.3 mL of 2-aminoethanol (99.0%) under stirring. The pH of the solution was adjusted to 7.0 by adding citric acid monohydrate (99.5%). All of the chemicals used here were purchased from Wako Pure Chemical Ind., Ltd. After the solution was left at 278 K for 3 weeks, pale yellow crystals were obtained. The crystals were identified by means of IR spectra and powder X-ray diffraction patterns.

In the calorimetric measurement, these crystals were packed into a bag made of polyethylene terephthalate (PET) to avoid reaction with the sample cell made of copper. This bag was then loaded into the sample cell. The dead space of the PET bag and sample cell were filled with helium gas to enhance thermal equilibration at low temperatures. The masses of the sample and PET were 2.7056 g (0.007 059 2 mol) and 0.0285 g, respectively.

The heat capacity of $Cd(H_2O)_2Ni(CN)_4\cdot 4H_2O$ was measured in the temperature range between 5 and 300 K using an adiabatic calorimeter described elsewhere.[16] The heat capacity measurement was carried out by standard intermittent heating method, i.e., repetition of equilibration and energizing intervals. The temperature increment for each measurement was between 0.5 and 2.5 K. It took about 30 s for the sample and cell to reach thermal equilibrium after each energy input around 5 K and about 5 min around 300 K. The accuracy of the heat capacity measurement was better than 0.5% at T < 15 K, 0.2% at 15 < T < 30 K, and 0.1% at T > 30 K.

In the calorimetric measurement, the temperature was measured using a Rh−Fe resistance thermometer (27 Ω at 273 K, purchased from Oxford Instruments Company) calibrated on the temperature scale EPT76 (T < 30 K) and IPTS68 (T > 30 K). The heat capacity difference caused by the conversion to the new temperature scale ITS90[17] was estimated to be smaller than 0.05% over the 14 K to 300 K temperature range.

For dielectric measurement, the sample crystals were ground on a mortar and shaped into a disk by applying pressure of about 300 MPa. The diameter and thickness of the disk were 13.00 and 0.760 mm, respectively. The mass density of the disk was 1.93 g cm^{-3}, which is almost the same as the density (1.93 g cm^{-3}) determined by single-crystal X-ray diffraction.[13,14] For electrodes, two circular pieces of gold foil with diameter of 10.09 mm was attached with a thin layer of Apiezon N-grease on both sides of the sample disk. The disk was mounted in a double thermostated environment in a cryostat. The sample temperature was stabilized to 0.03 K with an accuracy of 0.1 K. The capacitance was measured with an LCR meter (HP4284A-Hewlett Packard) in the frequency range between 20 Hz and 1 MHz and in the temperature range of 150−285 K. The measurement was performed in the heating direction as in the case of heat capacity measurement.

3. Results and Discussion

A. Heat Capacity. The molar heat capacities of $Cd(H_2O)_2Ni(CN)_4\cdot 4H_2O$ are collected in Table 1 and also plotted in Figure 1. No large thermal anomaly was observed over the temperature range examined. The present compound is different from $SnCl_2\cdot 2H_2O$ and $Cu(HCO_2)_2\cdot 4H_2O$ with respect to a cooperative ordering process (typically a phase transition) of the hydrogen atoms in the network.

B. Glass Transition. The quantity C_p/T, which helps one to find a slight C_p anomaly by offsetting the natural C_p increase with increasing temperature, was plotted as a function of temperature in Figure 2. In this plot, a small jump, corresponding to 0.5% of the total heat capacity, was found around 120 K. Figure 3 shows the spontaneous temperature drift rates

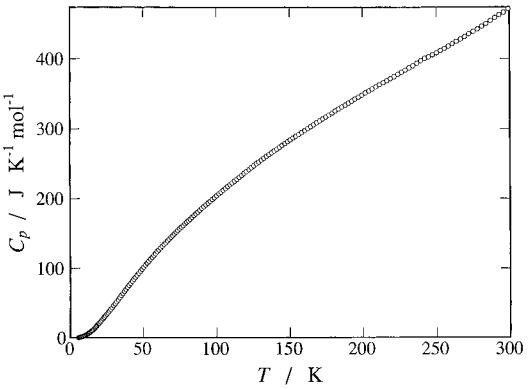

Figure 1. Molar heat capacity of $Cd(H_2O)_2Ni(CN)_4 \cdot 4H_2O$.

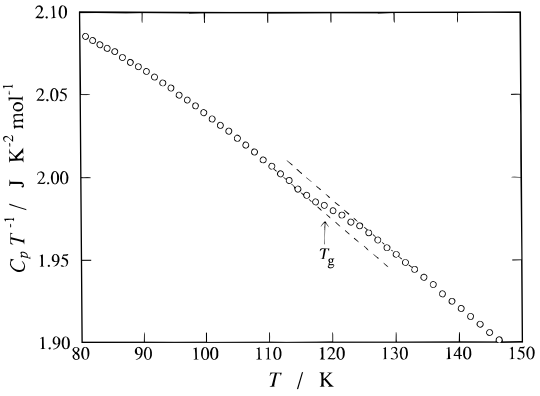

Figure 2. C_p/T plot of $Cd(H_2O)_2Ni(CN)_4 \cdot 4H_2O$ around the glass transition temperature.

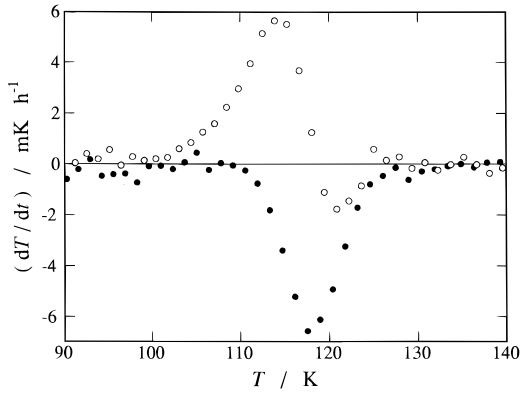

Figure 3. Spontaneous temperature drift rate of $Cd(H_2O)_2Ni(CN)_4 \cdot 4H_2O$ around the glass transition temperature: ○, quenched sample; ●, annealed sample.

observed at 1 min after each energy input of the heat capacity measurement; this quantity should be zero in the adiabatic calorimetry if no thermal anomaly happens. In the sample cooled continuously at the rate of 6 K min^{-1} (corresponding to the results in Figures 1 and 2), an exothermic drift followed by an endothermic one appeared in the temperature range 100−125 K. On the other hand, in the sample annealed at 110 K for 43 h, only an endothermic drift appeared starting at the annealing temperature. This type of temperature drift, which accompanies the heat capacity jump and depends on the thermal history of the sample, is one of the characteristic features of a glass transition.[18−20] The exothermic and endothermic drifts are due to the relaxation of configurational enthalpy which is related to the molecular motion frozen in at the glass transition. The glass transition temperature T_g was determined to be 120 K by taking the temperature where the temperature drift rate changed from positive to negative in the continuously cooled sample; this is the usual way to determine T_g in the adiabatic calorimetry.

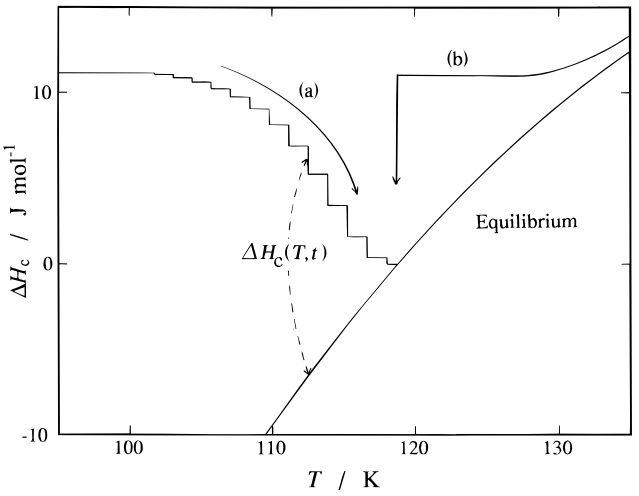

Figure 4. Temperature dependence of the configurational enthalpy of $Cd(H_2O)_2Ni(CN)_4 \cdot 4H_2O$. The arrows a and b represent the paths of the normal heat capacity measurement and the temperature jump experiment, respectively (see text for the details).

Figure 4 shows the diagram of the configurational enthalpy related to the glass transition. The steplike line represents the enthalpy path determined from the actual heat evolution experienced during the heat capacity measurement of the continuously cooled sample. The horizontal segment represents the temperature increase caused by supplying energy and the vertical one the exothermic enthalpy relaxation. The latter quantity was determined from

$$\Delta H_c(T,t) = \sum (\mathrm{d}T/\mathrm{d}t) C_p(\mathrm{total}) \Delta t \qquad (1)$$

where (dT/dt) is the same quantity as plotted in Figure 3, C_p(total) the heat capacity including that of the sample cell, and Δt the time between the midpoints of two successive energy input intervals (about 20 min). The arrow a (Figure 4) represents the directions in which the heat capacity measurement was carried out. The curve smoothly rising up to the right gives the hypothetical equilibrium configurational enthalpy derived by integrating the heat capacity difference between the two dashed lines drawn in Figure 2. The zero of ΔH_c was taken at the temperature at which the temperature drift rate of the continuously cooled sample passes through zero.

We conclude that the origin of the glass transition observed around 120 K is the freezing of the reorientational motion of the water molecules in the two-dimensional network of $Cd(H_2O)_2Ni(CN)_4 \cdot 4H_2O$ crystal since any other relaxational motion does not exist in this crystal. The excess heat capacity above T_g, corresponding to the enthalpy change of the equilibrium line in Figure 4, is due to the short-range ordering of the water orientation. The hypothetical (long-range) ordering transition should take place below T_g if the sample were cooled infinitely slowly. The present case is similar to those of hexagonal[21] and cubic[22] ices and various clathrate hydrates[23−26] with regard to the relation between the glass transition and hypothetical phase transition. Our conclusion will be confirmed by the result of the dielectric experiment described bellow.

C. Temperature Jump Method. To investigate the relaxation function and the relaxation times more precisely, the calorimetric experiment which we call the temperature jump was performed around T_g. The sample was cooled rapidly (ca. 6 K min^{-1}) from about 145 K down to a temperature around T_g. The temperature evolution caused by the exothermic effect due to the enthalpy relaxation was then measured under adiabatic condition until the sample reached the equilibrium state. The

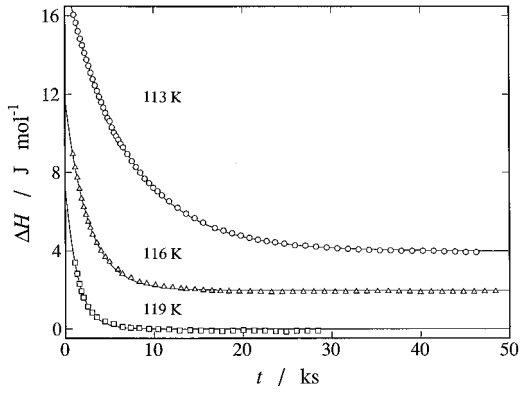

Figure 5. Enthalpy relaxation after the temperature jump around the glass transition temperature of $Cd(H_2O)_2Ni(CN)_4\cdot 4H_2O$. The curves are the exponential function determined by the least-squares fitting (see text for the details).

temperature evolution data $T(t)$ was converted to the configurational enthalpy relaxation data $H_c(t)$ by multiplying the heat capacity including that of the sample cell; the temperature dependence of the heat capacity can be neglected since the total temperature increase is small (0.02−0.05 K). This experiment was schematically shown by the arrow b in Figure 4. The experiments were carried out at several temperatures around T_g (113, 116, 119, and 121K). Some of the results are shown in Figure 5. The data at 116 and 113 K are shifted upward by 2 and 4 J mol^{-1}, respectively, for the sake of clarity. The relaxation curves are clearly temperature dependent.

D. Enthalpy Relaxation Time. In most of ice polymorphs and hydrate systems, the Debye type relaxation is useful as the first approximation.[21−26] In this case, the enthalpy relaxation process is represented by an exponential form

$$\Delta H_c(T,t) = \Delta H_c(T,0)\exp[-t/\tau(T)] \qquad (2)$$

where $\tau(T)$ is the relaxation time as a function of temperature. The enthalpy relaxation rate is given by differentiating eq 2 with respect to t to be

$$d\Delta H_c(T,t)/dt = -\Delta H_c(T,t)/\tau(T) \qquad (3)$$

In the temperature range far below T_g, where τ is long compared with the period required for one cycle of the heat capacity measurement (ca. 20 min), the relaxation rate can be regarded as a constant over this time and, therefore, the enthalpy relaxation times were calculated by eq 3. $d\Delta H_c(T,t)/dt$ and $\Delta H_c(T,t)$ were both obtained from the data in Figure 3. For the temperature jump data in which the duration of the experiment was more than 5 times longer than τ, the data were fitted to eq 2 by regarding $\Delta H_c(T,0)$ and τ as adjustable parameters. The data were actually fitted well to eq 2 as shown by the curves in Figure 5. The enthalpy relaxation times thus obtained will be discussed in section 3.F.

E. Dielectric Relaxation. Figure 6 shows the temperature dependence of the real (upper) and imaginary (lower) parts of the dielectric permittivity of $Cd(H_2O)_2Ni(CN)_4\cdot 4H_2O$ crystal. The dielectric dispersion was found in the temperature range 160−270 K. This dielectric dispersion arises from the reorientational motion of the water molecules, the only possible mode of dipole fluctuation in this crystal. The relaxation intensity (ca. 12 at 200 K) is smaller than the relaxation intensities of ice and clathrate hydrates (50−100) because the number density of H_2O molecules in this crystal is much smaller than those of ice and clathrate hydrates.

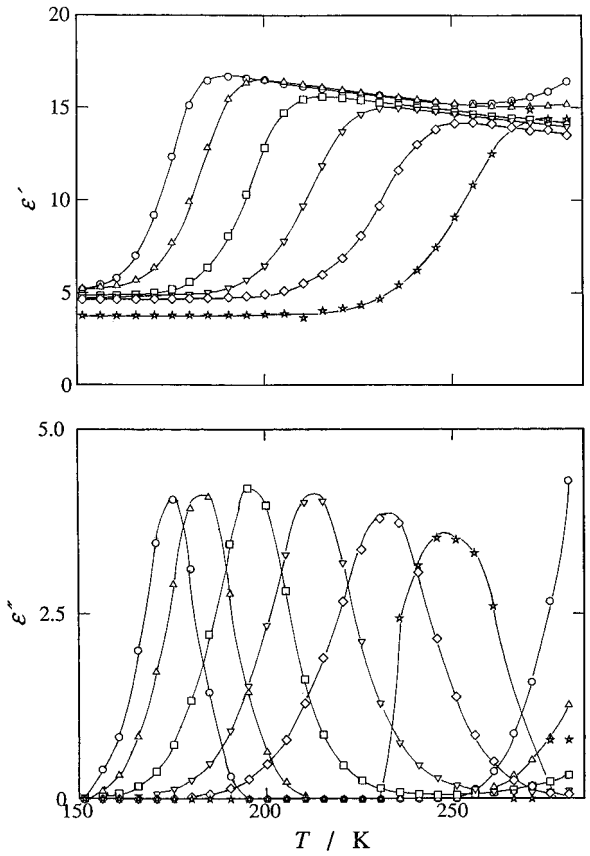

Figure 6. Temperature dependence of the real (upper) and imaginary (lower) parts of the dielectric permittivity of $Cd(H_2O)_2Ni(CN)_4\cdot 4H_2O$: ○, 20 Hz; △, 100 Hz; □, 1 kHz; ▽, 10 kHz; ◇, 100 kHz; ☆, 1 MHz.

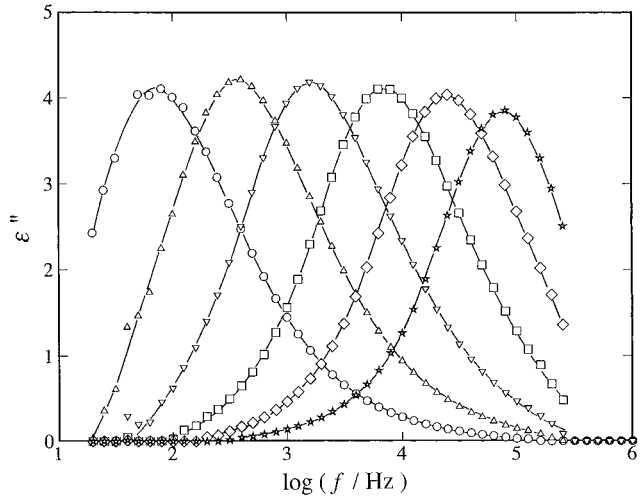

Figure 7. Frequency dependence of the imaginary parts of the dielectric permittivity of $Cd(H_2O)_2Ni(CN)_4\cdot 4H_2O$ at 180 (○), 190 (△), 200 (▽), 210 (□), 220 (◇) and 230 K (☆).

Figure 7 shows the frequency dependence of $\epsilon''$of the dielectric permittivity at six selected temperatures between 180 and 235 K. The dielectric relaxation times were determined from the peak frequencies of these plots by using the relation

$$\tau = 1/(2\pi f) \qquad (4)$$

Figure 8 shows the Cole−Cole plot of the data taken at 200 K. The data was fitted by the Cole−Cole function[27] as shown by the curve in this figure. The fitted non-Debye parameter α was 0.8 ($\alpha = 1$ for the Debye relaxation). This value did not depend much on the temperature. The relaxation function of

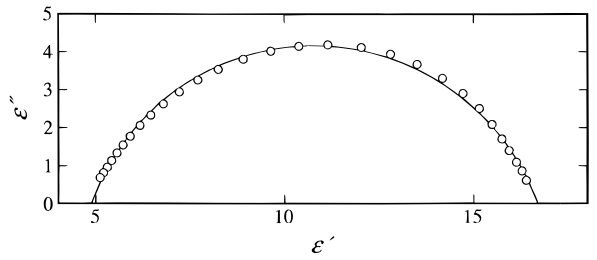

Figure 8. Cole−Cole plot for the complex dielectric permittivity of $Cd(H_2O)_2Ni(CN)_4{\cdot}4H_2O$ at 200 K. The curve was drawn by the Cole−Cole formula determined by the least-squares fitting (see text for the details).

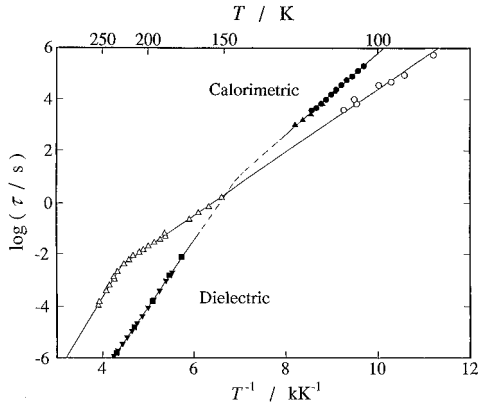

Figure 9. Arrhenius plot of the relaxation times of $Cd(H_2O)_2Ni(CN)_4{\cdot}4H_2O$ (closed symbols) and hexagonal ice (open symbols).[19,25] See text for the further description on the symbols. The straight lines are drawn by the least-squares fitting as described in the text.

the water reorientation is thus non-Debye but not much different from the Debye single τ type. This result may be consistent with the fact that the enthalpy relaxation data could be fitted approximately by the exponential (Debye) function.

F. Temperature Dependence of the Water Reorientation Rate. Figure 9 shows the Arrhenius plot for all of the relaxation times obtained in this study (closed symbols). The data on hexagonal ice (open symbols)[21,28] are also plotted for comparison. The data longer than 10^2 s were obtained from the enthalpy relaxation and those shorter than 1 s from the dielectric relaxation. The closed circles and triangles were obtained from eqs 3 and 2, respectively. The closed squares and inverted triangles were from the T vs ϵ'' and f vs ϵ'' plots, respectively. The relaxation times obtained in this study are all considered to be for the reorientational motion of water molecules in the two-dimensional hydrogen bond system as described before. The calorimetric and dielectric data follow the Arrhenius type temperature dependence with different slopes (activation energy). The two extrapolated straight lines intersect as Figure 9 shows. The intersection has been actually observed in hexagonal ice.[28]

G. Defect Model. In hexagonal ice, the reorientation of the water molecules takes place as the result of the transfer of the L (no proton on a O−O bond) and D (two protons on a O−O bond) defects.[29] There are two different types of defects in ice. One is the intrinsic orientational defect (Bjerrum defect) that is a neutral pair of L and D defects produced by a rotation of a water molecule.[30] The number of this type of defects (n_{in}) activated increases with temperature as given by

$$n_{in} = n_0 \exp(-\Delta E_f/RT) \qquad (5)$$

where ΔE_f is the activation energy of the defect formation and n_0 the total number of water molecules. The other is the extrinsic impurity defect, which is sometimes neutral and sometimes charged and sometimes L and sometimes D. The number of this defect (n_{ex}) is of course independent of temperature and much smaller than n_0. By assuming that the activation energy of the defect transfer (ΔE_t) does not depend on defect type, the frequency of the water reorientation f, which is inverse of the relaxation time τ, is given by

$$f = 1/\tau = [(n_{in} + n_{ex})/n_0][f_0 \exp(-\Delta E_t/RT)] \qquad (6)$$

Here f_0 is the frequency factor assumed to be the same for the extrinsic and intrinsic defects. From eqs 5 and 6, τ is approximated to be the following Arrhenius forms with different activation energies at higher and lower temperature limits:

$$\tau = (1/f_0) \exp[(\Delta E_f + \Delta E_t)/RT]$$
$$(n_{in} \gg n_{ex} \text{ at high temperature}) \qquad (7)$$

$$\tau = (n_0/n_{ex}f_0) \exp(\Delta E_t/RT)$$
$$(n_{in} \ll n_{ex} \text{ at low temperature}) \qquad (8)$$

The temperature dependence of the relaxation time in hexagonal ice, which exhibits a bend around 230 K, is fully explained by this model. ΔE_f and ΔE_t were determined by the least squares fitting to be 32.8 and 23.4 kJ mol^{-1}, respectively.

We have applied this model to the water reorientation of $Cd(H_2O)_2Ni(CN)_4{\cdot}4H_2O$ crystal. The calorimetric and dielectric data sets were fitted well by two different straight lines as shown in Figure 7. ΔE_f and ΔE_t were determined to be 18.3 and 30.3 kJ mol^{-1}, respectively. ΔE_f of the present sample (18.3 kJ mol^{-1}) is remarkably smaller than that of hexagonal ice (32.8

TABLE 2: Molar Themodynamic Functions of $CdNi(H_2O)_2(CN)_4{\cdot}4H_2O$ Crystal (M = 383.27 g mol^{-1}, R = 8.314 51 J K^{-1} mol^{-1}, $\Phi_m^\circ = \Delta_0^T S_m^\circ - \Delta_0^T H_m^\circ/T$)

T/K	$C_{p,m}^\circ/R$	$\Delta_0^T H_m^\circ/TR$	$\Delta_0^T S_m^\circ/R$	Φ_m°/R
5	0.05074	0.01264	0.01684	0.004 204
10	0.4111	0.1025	0.1365	0.03397
15	1.285	0.3377	0.4522	0.1145
20	2.571	0.7285	0.9903	0.2617
25	4.079	1.245	1.723	0.4779
30	5.692	1.851	2.608	0.7573
40	8.991	3.226	4.701	1.474
50	12.11	4.692	7.043	2.351
60	15.01	6.174	9.512	3.338
70	17.64	7.627	12.03	4.399
80	20.07	9.032	14.54	5.510
90	22.36	10.39	17.04	6.652
100	24.52	11.69	19.51	7.814
110	26.57	12.95	21.94	8.988
120	28.59	14.17	24.34	10.17
130	30.55	15.36	26.71	11.35
140	32.35	16.51	29.04	12.53
150	34.09	17.62	31.33	13.71
160	35.77	18.70	33.58	14.88
170	37.38	19.75	35.80	16.04
180	38.95	20.78	37.98	17.20
190	40.48	21.77	40.13	18.35
200	41.96	22.75	42.24	19.49
210	43.41	23.70	44.32	20.63
220	44.88	24.63	46.38	21.75
230	46.35	25.54	48.41	22.87
240	47.79	26.44	50.41	23.97
250	49.18	27.32	52.39	25.07
260	50.57	28.19	54.34	26.16
270	52.04	29.04	56.28	27.24
273.15	52.53	29.31	56.89	27.58
280	53.62	29.89	58.20	28.31
290	55.23	30.74	60.11	29.37
298.15	56.60	31.42	61.66	30.23
300	56.94	31.58	62.01	30.43

kJ mol^{-1}). We suppose that this is the effect of the protons pointing out of the H_2O layer and not engaged in-layer hydrogen bonding, i.e., the energy to disrupt a hydrogen bond is not required for this proton. Finally, the relative concentration of the extrinsic defects was $n_{ex}/n_0 = 4 \times 10^{-5}$, which is equivalent to one defect for every 25 000 water molecules. Here we assume $f_0 = 10^{13}$ s^{-1}.

4. Conclusions

We have found a glass transition due to the freezing of the reorientational motion of the water molecules at 120 K. The reorientational relaxation times were obtained from the enthalpy relaxation data below and around the glass transition (105−120 K) and from the dielectric relaxation data in the temperature range 150−285 K. The relaxation function was non-Debye but not much different from the Debye single τ type. Calorimetric and dielectric relaxation times lie on separate smooth lines in the wide time scale over $10^{-6}-10^{6}$ s in the Arrhenius plot. The water reorientational motion could be analyzed by the model considering the formation and transfer of the Bjerrum defect as in the case of the three-dimensional ice polymorphs.

Appendix

Standard Thermodynamic Functions. The molar heat capacity, enthalpy, entropy, and Giauque function of $Cd(H_2O)_2Ni(CN)_4\cdot 4H_2O$ crystal were calculated from the smoothed heat capacity data and summarized in Table 2. Extrapolation of the heat capacity down to 0 K was performed by using the following odd-order polynomial function.

$$C_p/(\mathrm{J\ K^{-1}\ mol^{-1}}) = 3.33 \times 10^{-3}(T/\mathrm{K})^3 + 2.16 \times 10^{-6}(T/\mathrm{K})^5 - 1.27 \times 10^{-8}(T/\mathrm{K})^7$$

References and Notes

(1) Falk, M.; Knop, O. *Water: A Comprehensive Treatise*; Franks, F., Ed.; Plenum Press: New York, 1973; Vol. 2, Chapter 2.
(2) Matsuo, T.; Suga, H. *Rev. Inorg. Chem.* **1981**, *3*, 371.
(3) Kiriyama, H.; Kitahama, K.; Nakamura, O.; Kiriyama, R. *Bull. Chem. Soc. Jpn.* **1973**, *46*, 1389.
(4) Kiriyama, K.; Kiriyama, H. *Bull. Chem. Soc. Jpn.* **1977**, *50*, 3167.
(5) Kiriyama, K.; Ibamoto, H.; Matsuo, K. *Acta Crystallogr.* **1954**, *7*, 482.
(6) Okada, K.; Kay, M. I.; Cromer, D. T.; Almodovar, I. *J. Chem. Phys.* **1966**, *44*, 1648.
(7) Bernal, J. D.; Fowler, R. H. *J. Chem. Phys.* **1933**, *1*, 525.
(8) Matsuo, T.; Tatsumi, M.; Suga, H.; Seki, S. *Solid State Commun.* **1973**, *13*, 1829.
(9) Matsuo, T.; Oguni, M.; Suga, H.; Seki, S.; Nagle, J. F. *Bull. Chem. Soc. Jpn.* **1974**, *47*, 57.
(10) Tatsumi, M.; Matsuo, T.; Suga, H.; Seki, S.; Nagle, J. F. *Bull. Chem. Soc. Jpn.* **1979**, *52*, 728.
(11) Tatsumi, M.; Matsuo, T.; Suga, H.; Seki, S.; Nagle, J. F. *Bull. Chem. Soc. Jpn.* **1979**, *52*, 716.
(12) Matsuo, T.; Kume, Y.; Suga, H.; Seki, S. *J. Phys. Chem. Solids* **1976**, *37*, 499.
(13) Ham, W. K.; Weakley, T. J. R.; Page, C. J. *J. Solid State Chem.* **1993**, *107*, 101.
(14) Park, K. -M.; Kuroda, R.; Iwamoto, T. *Angew. Chem., Int. Ed. Engl.* **1993**, *32*, 884.
(15) Booth, H. S., Ed. *Inorganic Syntheses*; McGraw-Hill Book Co.: New York, 1946; Vol. II, p 227.
(16) Yamamuro, O.; Oguni, M.; Mastuo, T.; Suga, H. *Bull. Chem. Soc. Jpn.* **1987**, *60*, 1269.
(17) Goldberg, R. N.; Weir, R. D. *Pure Appl. Chem.* **1992**, *64*, 1545.
(18) Suga, H.; Seki, S. *J. Non-Cryst. Solids* **1974**, *16*, 171.
(19) Suga, H.; Seki, S. *Faraday Discuss. R. Soc. Chem.* **1981**, *69*, 221.
(20) Suga, H. *J. Chim. Phys. Phys.-Chim. Biol.* **1985**, *82*, 275.
(21) Haida, O.; Matsuo, T.; Suga, H.; Seki, S. *J. Chem. Thermodyn.* **1974**, *6*, 815.
(22) Yamamuro, O.; Oguni, M.; Matsuo, T.; Suga, H. *J. Phys. Chem. Solids* **1987**, *48*, 935.
(23) Yamamuro, O.; Oguni, M.; Matsuo, T.; Suga, H. *J. Phys. Chem. Solids* **1988**, *49*, 425.
(24) Yamamuro, O.; Handa, Y. P.; Oguni, M.; Suga, H. *J. Inclusion Phenom.* **1990**, *8*, 45.
(25) Kuratomi, N.; Yamamuro, O.; Matsuo, T.; Suga, H. *J. Chem. Thermodyn.* **1991**, *23*, 485.
(26) Yamamuro, O.; Suga, H. *J. Therm. Anal.* **1989**, *35*, 2025.
(27) Cole, K. S.; Cole, R. H. *J. Chem. Phys.* **1941**, *9*, 341.
(28) Kawada, S.; Dohata, H. *J. Phys. Soc. Jpn.* **1985**, *54*, 477.
(29) Fletcher, N. H. *The Chemical Physics of Ice*; Cambridge University Press: Cambridge, 1970.
(30) Bjerrum, N. *Science* **1952**, *115*, 385.